Angela Bonaccorso

INFN PISA
Istituto Nazionale di Fisica Nucleare
Sezione di Pisa

ECT*, Trento June 2024

How to find (THE/A?) optical potential for knockout reactions

In collaboration with Imane Moumene, Dep. of Phyisics, Bratislava.

Used opt mod code SIDES, Guillauma Blanchon et al.

Comput.Phys.Commun. 254 (2020) 107340.

Road to Heaven or Tears in Haven? (Lionel Reach vs Eric Clapton)

- Eikonal->S-matrix ->optical potential
- single folding vs phenomenological vs. double folding
- n-target,core-target
- ^{9}Be, ^{12}C most used targets
- Test: energy dependence of σ_R
- Phenomenological vs ab-initio

Historical background

PHYSICAL REVIEW C, VOLUME 61, 034605

Final state interaction effects in breakup reactions of halo nuclei

A. Bonaccorso*
Institute for Nuclear Theory, Seattle, Washington 98195-1550
and Istituto Nazionale di Fisica Nucleare, Sezione di Pisa, I-56100 Pisa, Italy†

F. Carstoiu
Institute of Atomic Physics, P.O. Box MG-6, Bucharest, Romania
(Received 1 October 1999; published 11 February 2000)

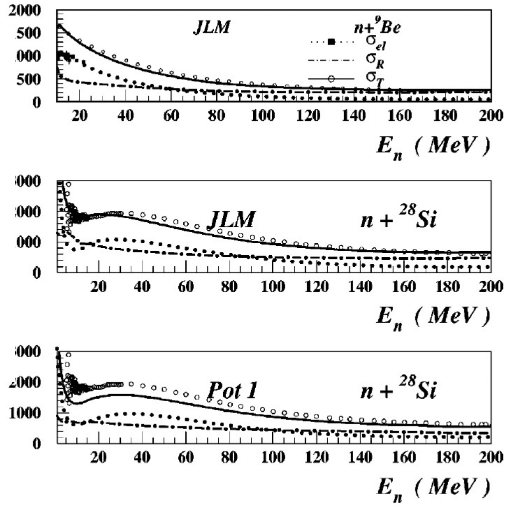

FIG. 1. Neutron-target cross sections as a function of the neutron incident energy. Top figure: ^{9}Be target. Dotted and dot-dashed curves are the elastic and reaction cross sections, respectively. Full curve is their sum. Data points from Ref. [18]. Center and bottom figure: ^{28}Si target with JLM potential and optical potential from Table I, respectively. Same notation as above. Data points from Ref. [18].

sorptive, and diffractive one neutron breakup cross sections from the halo orbital in ^{11}Be calculated from Eqs. (2.3) and (2.8) on the same targets and with the same n-target JLM optical potentials as Fig. 1. The initial state parameters used for the bound neutron in the ground state and core excited states of ^{11}Be, discussed in the following, are given in Table II. We have used the same single particle assignments and spectroscopic factors as in [6]. In the case of core excited states, each separation energy is the sum of the given state excitation energy plus the neutron separation energy in ^{11}Be.

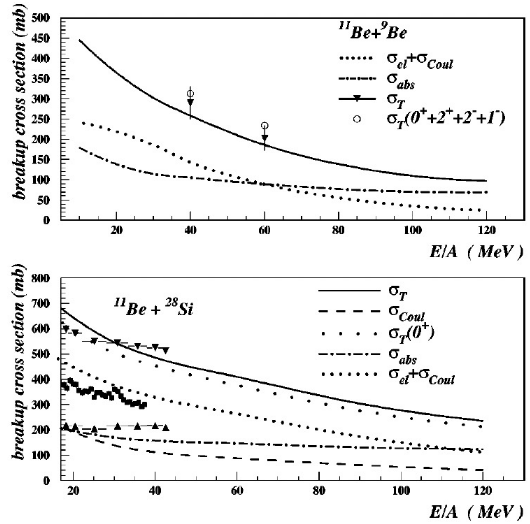

FIG. 2. Neutron breakup cross sections from ^{11}Be as a function of the incident energy per nucleon. Top figure: ^{9}Be target. Dotted and dot-dashed curves are the diffractive and absorptive breakup cross sections, respectively, from the halo orbital alone. Full curve is their sum. The full triangle symbol at 40A MeV is datum from Ref. [19], at 60A MeV from Ref. [21]. The open circles at the same energies are our total breakup cross sections including contributions from core states as given in Tables III and IV. Bottom figure: ^{28}Si target. Dashed line is the Coulomb breakup, dot-dashed line is the absorption cross section. Close dotted line is the sum of diffractive breakup and Coulomb breakup. The full curve is their sum. Core excited state contributions are included. Long dotted curve is the total breakup from the ^{11}Be halo orbital alone. Data points from Ref. [22]: the full squares are the data corresponding to neutrons detected in coincidence with the ^{10}Be core, due to Coulomb breakup and diffraction; the lower solid triangles are the data for absorption and the upper inverted triangles are the inclusive data.

ELSEVIER

Nuclear Physics A 706 (2002) 322–334

NUCLEAR PHYSICS A

www.elsevier.com/locate/npe

Optical potentials of halo and weakly bound nuclei

A. Bonaccorso[a,*], F. Carstoiu[b]

PHYSICAL REVIEW C **89**, 024619 (2014)

Optical potential for the n-^{9}Be reaction

Angela Bonaccorso[1] and Robert J. Charity[2]

Few-Body Syst (2016) 57:331–336
DOI 10.1007/s00601-016-1082-4

CrossMark

A. Bonaccorso · F. Carstoiu · R. J. Charity · R. Kumar
G. Salvioni

Differences Between a Single- and a Double-Folding Nucleus-^{9}Be Optical Potential

PHYSICAL REVIEW C **94**, 034604 (2016)

Imaginary part of the ^{9}C -^{9}Be single-folded optical potential

A. Bonaccorso,[1,*] F. Carstoiu,[2] and R. J. Charity[3]

Nuclear Physics A 1006 (2021) 122109

Localization of peripheral reactions and sensitivity to the imaginary potential

Imane Moumene[a,b], Angela Bonaccorso[c,*]

PHYSICAL REVIEW C **108**, 044609 (2023)

Optical potentials and nuclear reaction cross sections for n-^{12}C and N-^{12}C scattering

Imane Moumene[1,*] and Angela Bonaccorso[2,†]

and in preparation

Breakup (knockout) eikonal formulae

Finally following the derivation in [74] the EBU eikonal cross section in the no-recoil approximation is

Including kinematics

$$\frac{d\sigma_{EBU}}{dk_1} = \int d^2\mathbf{b}_C \, |S_{CT}(\mathbf{b}_C)|^2 \times \int d^2\mathbf{r}_{Cn_\perp} \, |1 - S_n(\mathbf{b}_n)|^2 \, |\tilde{\phi}_0(\mathbf{r}_{Cn_\perp}, k_1)|^2, \quad (24)$$

and the NEB formula [27,28]

$$\frac{d\sigma_{NEB}}{dk_1} = \int d^2\mathbf{b}_C \, |S_{CT}(\mathbf{b}_C)|^2 \times \int d^2\mathbf{r}_{Cn_\perp} \left(1 - |S_n(\mathbf{b}_n)|^2\right) |\tilde{\phi}_0(\mathbf{r}_{Cn_\perp}, k_1)|^2. \quad (25)$$

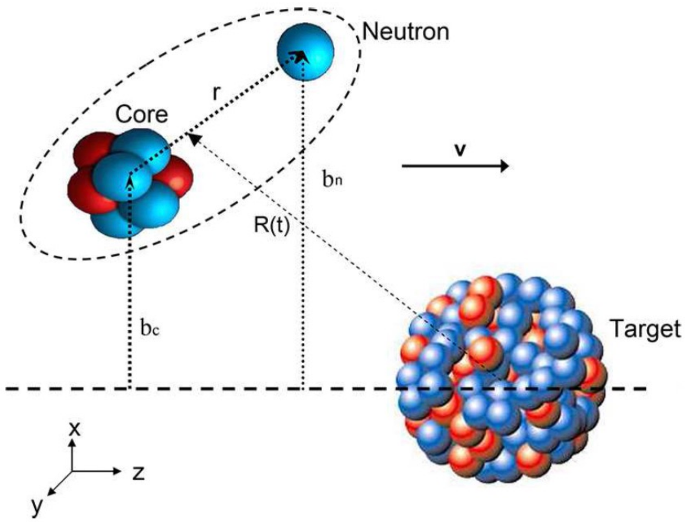

stripping

$$\sigma_{-n}^{inel} = \int d^2\mathbf{b_c} |S_{ct}(\mathbf{b_c})|^2 \int d^2\mathbf{r}_\perp (1 - |S_n(\mathbf{b_n})|^2) |\tilde{\phi}_0(\mathbf{r}_\perp)|^2$$

C²S

diffraction

$$\sigma^{el}_{-n} = \int \mathrm{d}^2\mathbf{b}_c |S_{ct}(\mathbf{b}_c)|^2 \int \mathrm{d}^2\mathbf{r}_\perp |1 - S_n(\mathbf{b}_n)|^2 |\tilde{\phi}_0(\mathbf{r}_\perp)|^2.$$

C²S

What really matters:

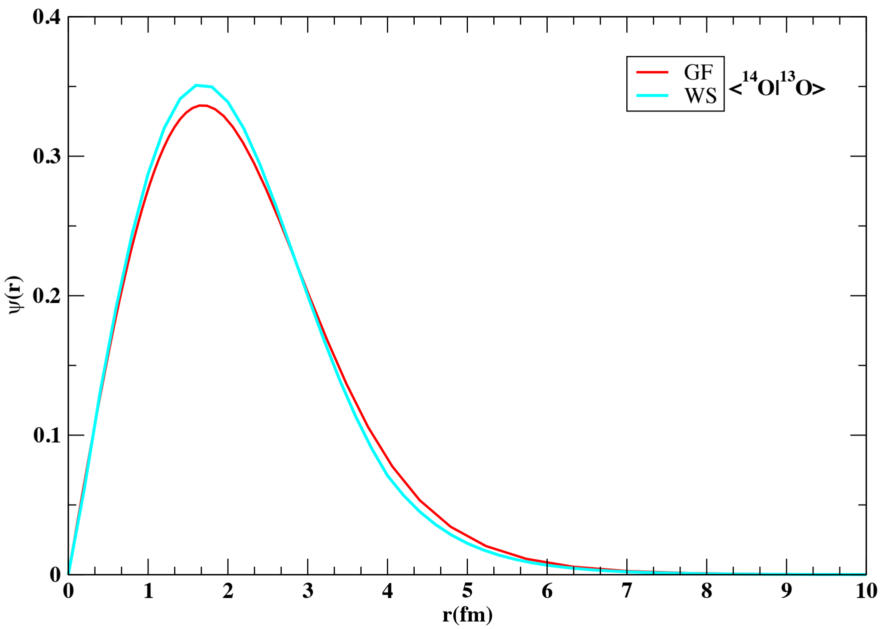

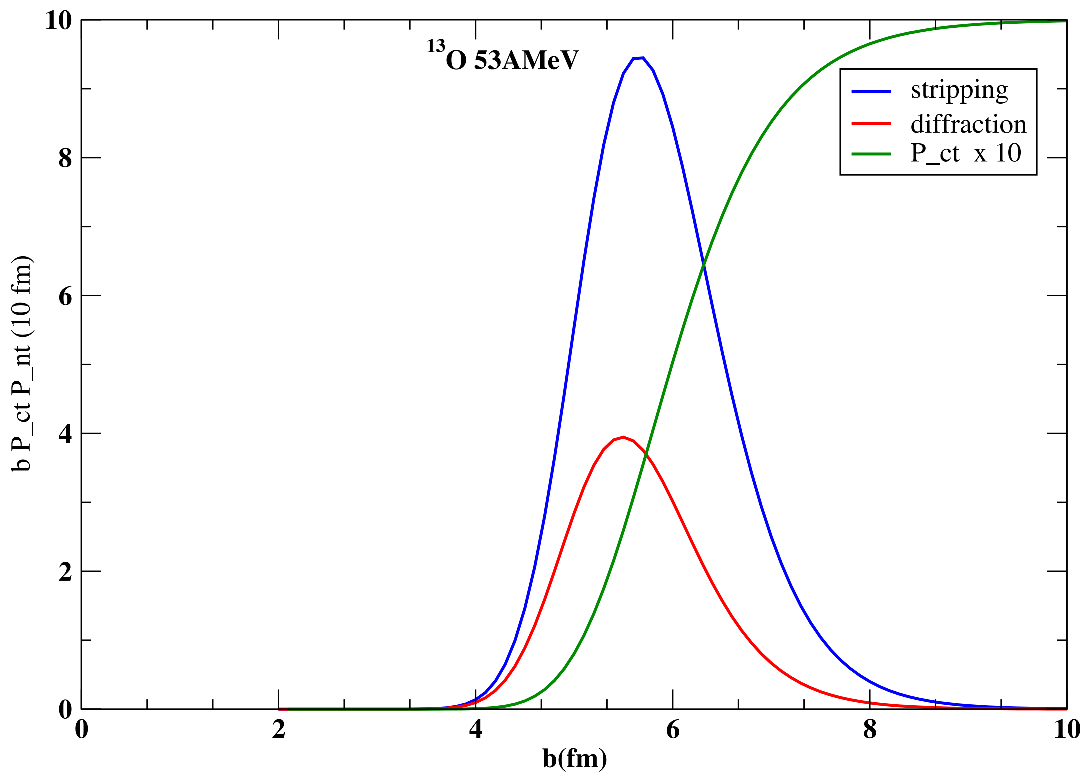

- Only the imaginary part of V_{ct} optical potential enters in the calculations of $|S_{ct}|^2$
- In 1- $|S_{nt}|^2$ (stripping) again only the imaginary part of V_{nt}
- In $|1- S_{nt}|^2$ both real and imaginary. However this term (elastic breakup) is usually << than the stripping term.

- Look for the best $W_{(nt,ct)}$ giving the best $|S_{(nt,ct)}|^2$ $\longrightarrow$ $\sigma^R_{(nt,ct)}$
- Fitting elastic angular distributions might be a bit of overwork in particular as at the energies we are intersted in >100AMeV $\sigma^R_{(nt,ct)} >> \sigma^{el}_{(nt,ct)}$

N+N The Glauber reaction cross section is given by

$$\sigma_R = 2\pi \int_0^\infty b db(1 - |S_{NN}(\mathbf{b})|^2), \quad (1)$$

where

$$|S_{NN}(\mathbf{b})|^2 = e^{2\chi_I(b)} \quad (2)$$

is the probability that the nucleus-nucleus (NN) scattering is elastic for a given impact parameter **b**.

The imaginary part of the eikonal phase shift is given by

$$\chi_I(\mathbf{b}) = \frac{1}{\hbar v}\int dz W^{NN}(\mathbf{b},z) = \frac{1}{\hbar v}\int dz \int d\mathbf{r_1} W^{nN}(\mathbf{r_1}-\mathbf{r})\rho(\mathbf{r_1}), \quad (3)$$

where W^{NN} is negative defined as

s.f.

$$W^{NN}(\mathbf{r}) = \int d\mathbf{b_1} W^{nN}(\mathbf{b_1}-\mathbf{b},z)\int dz_1 \rho(\mathbf{b_1},z_1). \quad (4)$$

d.f.

$$W^{NN}(\mathbf{r}) = -\frac{1}{2}\hbar v \sigma_{nn}\int d\mathbf{b_1}\rho_p(\mathbf{b_1}-\mathbf{b},z)\int dz_1 \rho_t(\mathbf{b_1},z_1). \quad (5)$$

Also

s.f.

$$W^{nN}(\mathbf{r}) = -\tfrac{1}{2}\hbar v \sigma_{nn}\rho_t(\mathbf{r}) \quad (6)$$

d.f.

$$\chi_I(\mathbf{b}) = -\frac{1}{2}\sigma_{nn}\int d\mathbf{b_1}\int dz\rho_p(\mathbf{b_1}-\mathbf{b},z)\int dz_1\rho_t(\mathbf{b_1},z_1).$$

The double folding (5) for $\mathbf{W^{NN}}$ is conceptually **wrong** because the interaction acts only to first order, infact it was originally introduced for the REAL part. Eq.(4) with a phenomenological W^{nN} is in principle more accurate.

PHYSICAL REVIEW C, VOLUME 62, 034608

Scatterings of complex nuclei in the Glauber model

B. Abu-Ibrahim* and Y. Suzuki

$$e^{i\tilde{\chi}_{\rm OLA}(\boldsymbol{b})} = \exp\left(-\int d\boldsymbol{r}\,\rho_P(\boldsymbol{r})\Gamma_{NT}(\boldsymbol{\xi}+\boldsymbol{b})\right),$$

$$\Gamma_{NT}(\boldsymbol{b}) = \sum_{k=1}^{K}\frac{1-i\alpha_k}{4\pi\beta_k}\sigma_k \exp\left(-\frac{\boldsymbol{b}^2}{2\beta_k}\right),$$

$$W_{\mathrm{MOL}}(\mathbf{r}) = \frac{1}{2}\hbar v\left(\sigma_1 \frac{e^{-r^2/2\beta_1}}{(2\pi\beta_1)^{3/2}} + \sigma_2 \frac{e^{-r^2/2\beta_2}}{(2\pi\beta_2)^{3/2}}\right).$$

TABLE I. Parameters of proton-^{12}C profile functions used in the present calculations, see Eq. (9). The total and reaction cross sections, σ_T and σ_R, calculated by the profile functions are also shown.

T_p (MeV)	σ_T (mb)	σ_R (mb)	σ (fm^2)	β (fm^2)	α
800	341	249	52.89	1.9702	−0.111 682
			−18.78	1.0735	0.0149455
398	285	221	32.303	2.117	0.0867
			−3.740	0.5204	0.4212
340	283	213	32.0	2.0	0.1
			−3.7	0.4	0.28
200	275	215	31.947	2.214	0.127
			−4.51	0.827	0.8852

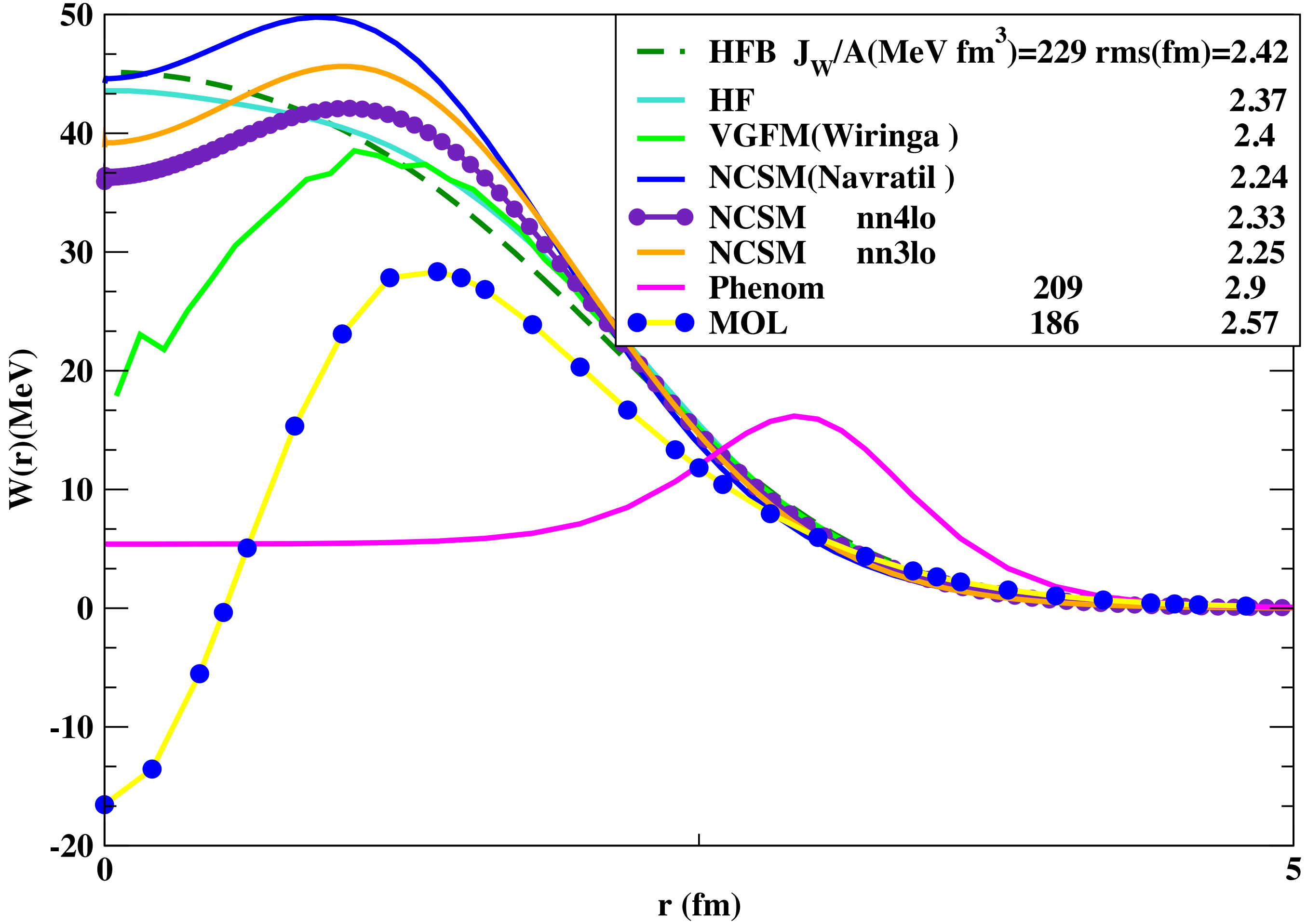

HFB J_W/A(MeV fm^3)=229 rms(fm)=2.42
HF 2.37
VGFM(Wiringa) 2.4
NCSM(Navratil) 2.24
NCSM nn4lo 2.33
NCSM nn3lo 2.25
Phenom 209 2.9
MOL 186 2.57
W(r)(MeV)
r (fm)

-^{12}C

INFN Angela Bonaccorso
Istituto Nazionale di Fisica Nucleare

A.B & R. J. Charity, PRC89, 024619 (2014) **Best n+^{9}Be O.P.**

Resonances described by $$\delta V(r) = 16\alpha \frac{e^{2(r-R^R)/a^R}}{(1+e^{(r-R^R)/a^R})^4}.$$ consistent with dispersive contribution

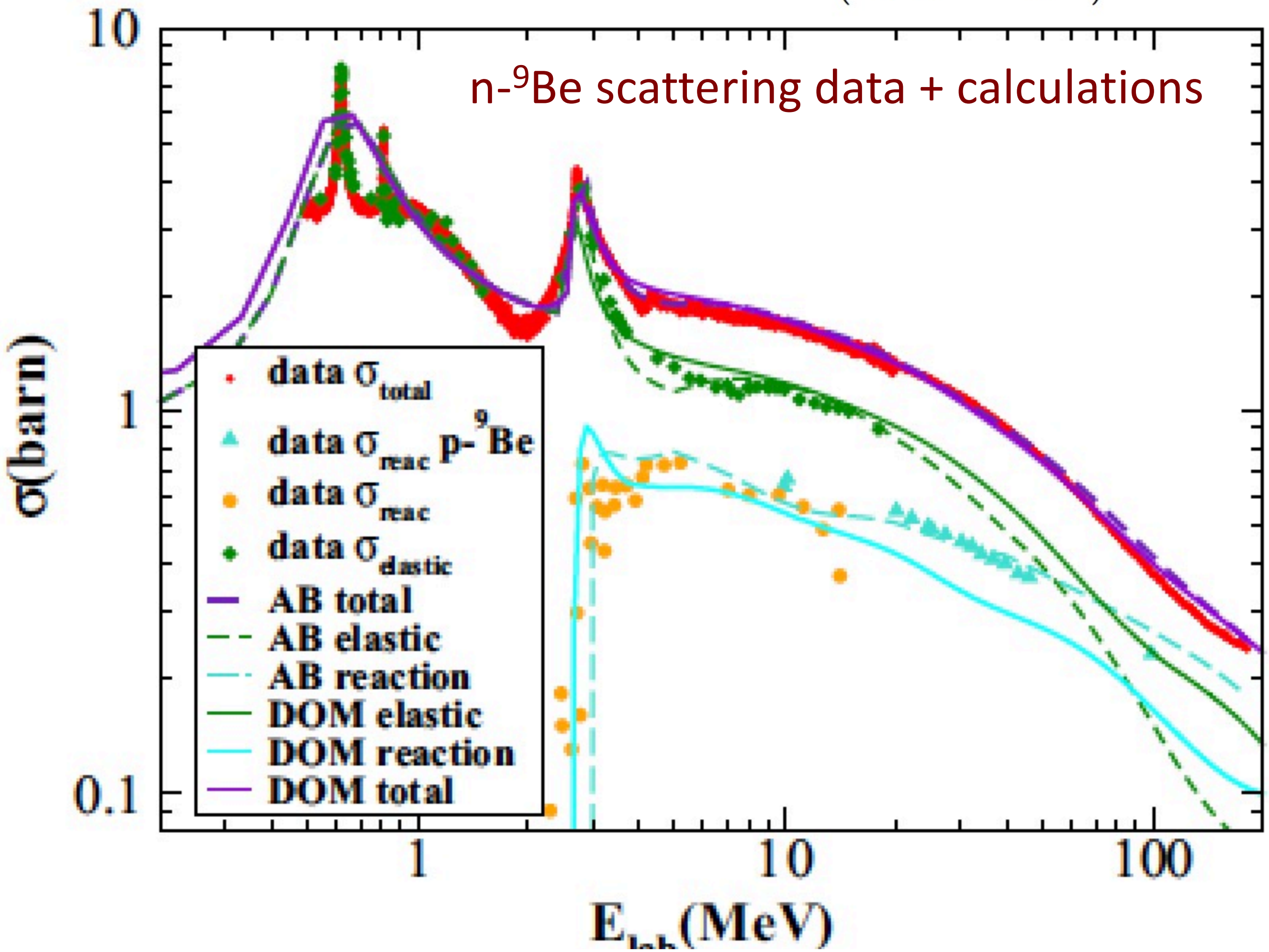

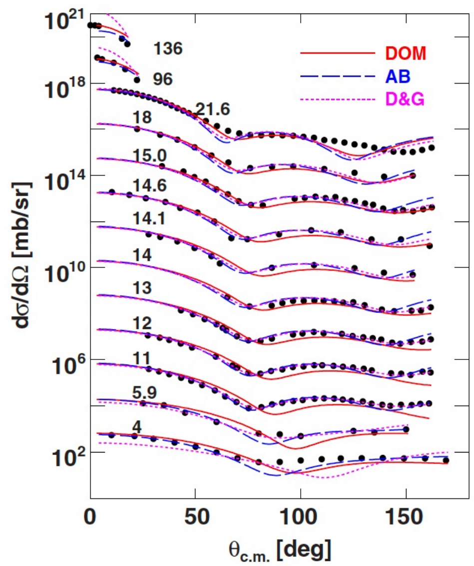

FIG. 2. (Color online) Fitted elastic-scattering angular distributions for $n + {}^9$Be with the dispersive optical model, the AB potential, and the Dave and Gould (DG) potential [19]. The experimental data are from Refs. [6,8,19,37–42]. For display purposes, the fits and data have been successively scaled by a further factor of 30 for each higher neutron energy. Curves and data are labeled by the neutron laboratory energy in MeV.

Total experimental and calculated cross sections. Lower blue symbols for ^{9}Be, upper red symbols for ^{12}C. The optical model calculations are given by the orange and cyan dashed lines, respectively. The solid green line is a calculation made with a DOM potential obtained for ^{12}C and applied to ^{9}Be. DOM calculations (LHS) curtesy of Mack Atkinson (LLNL)

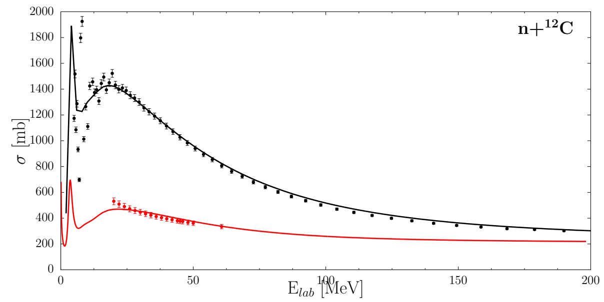

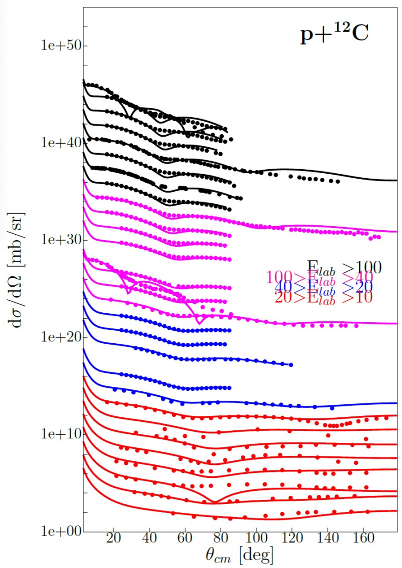

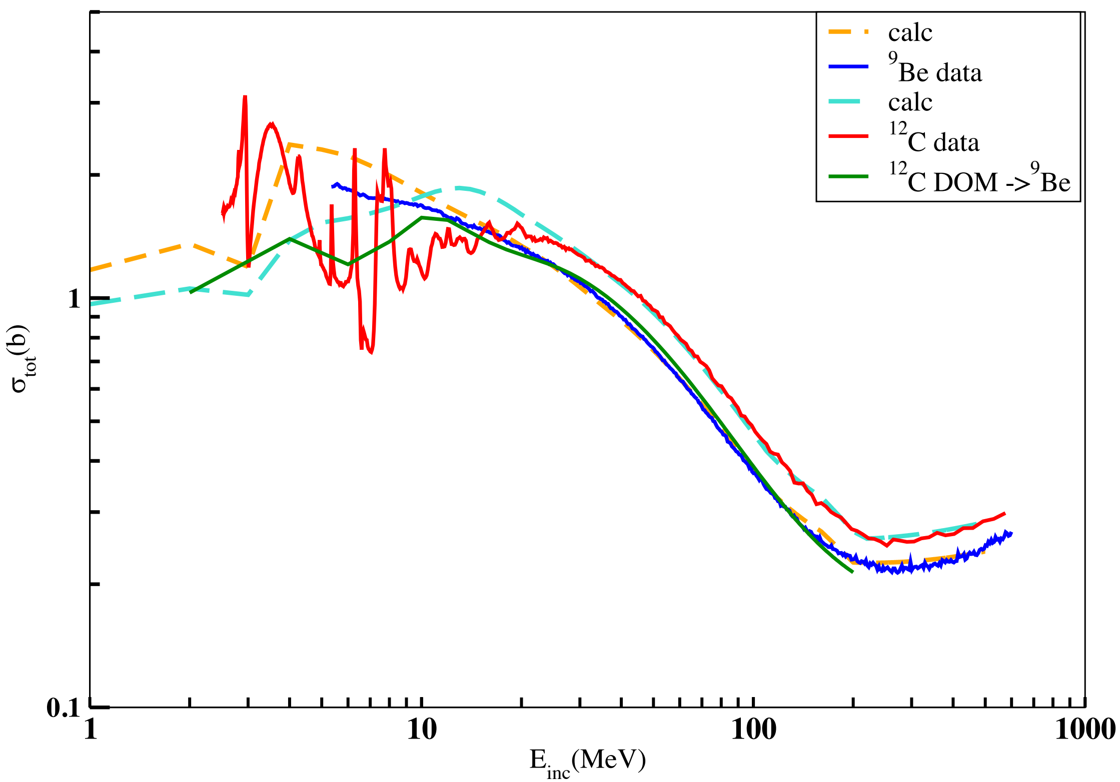

^{12}C

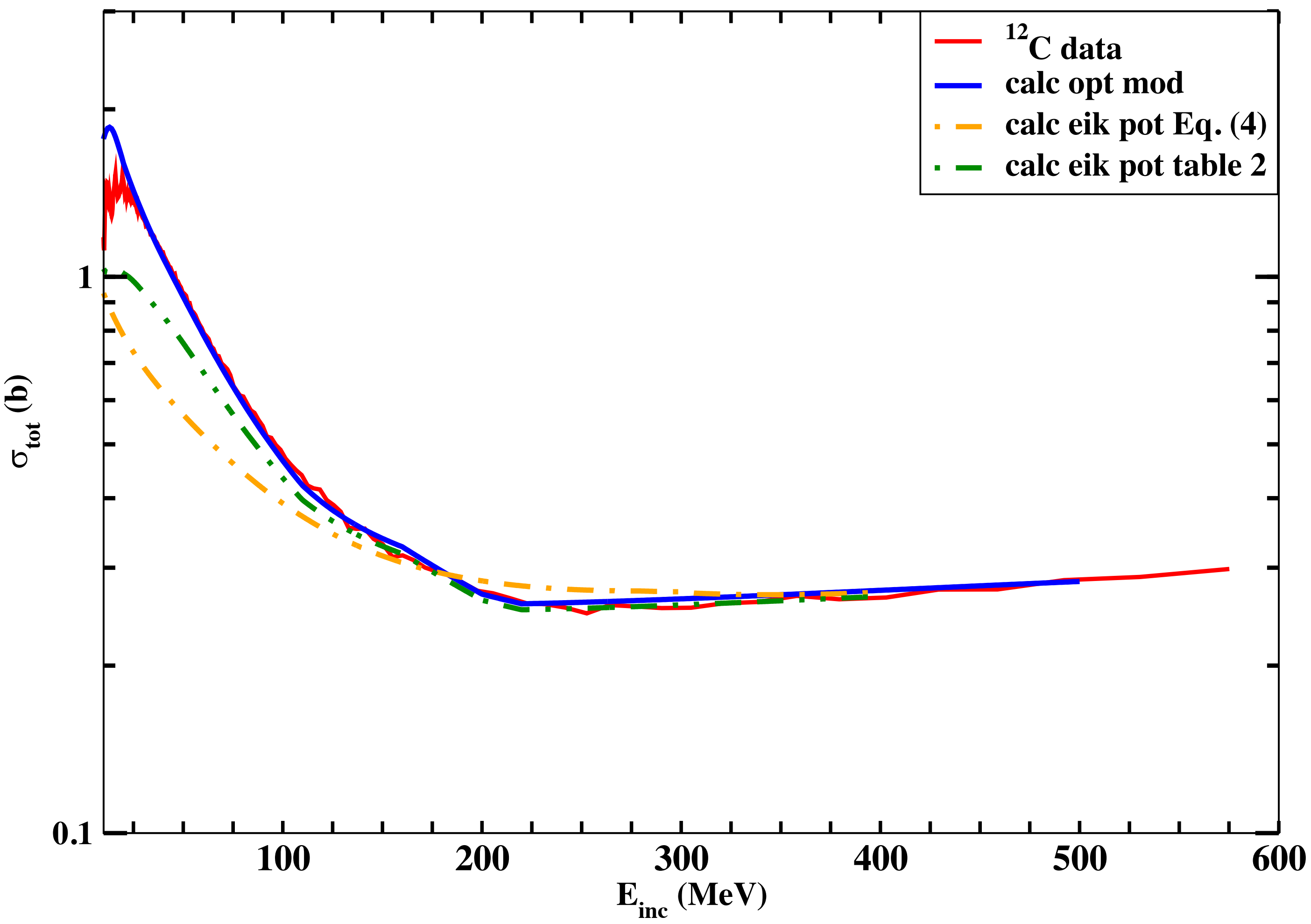

^{12}C data
calc opt mod
calc eik pot Eq. (4)
calc eik pot table 2
1
0.1
100
200
300
400
500
600
σ_{tot} (b)
E_{inc} (MeV)

PHYSICAL REVIEW C **108**, 044609 (2023)

Optical potentials and nuclear reaction cross sections for n-^{12}C and N-^{12}C scattering

Imane Moumene[1,*] and Angela Bonaccorso[2,†]

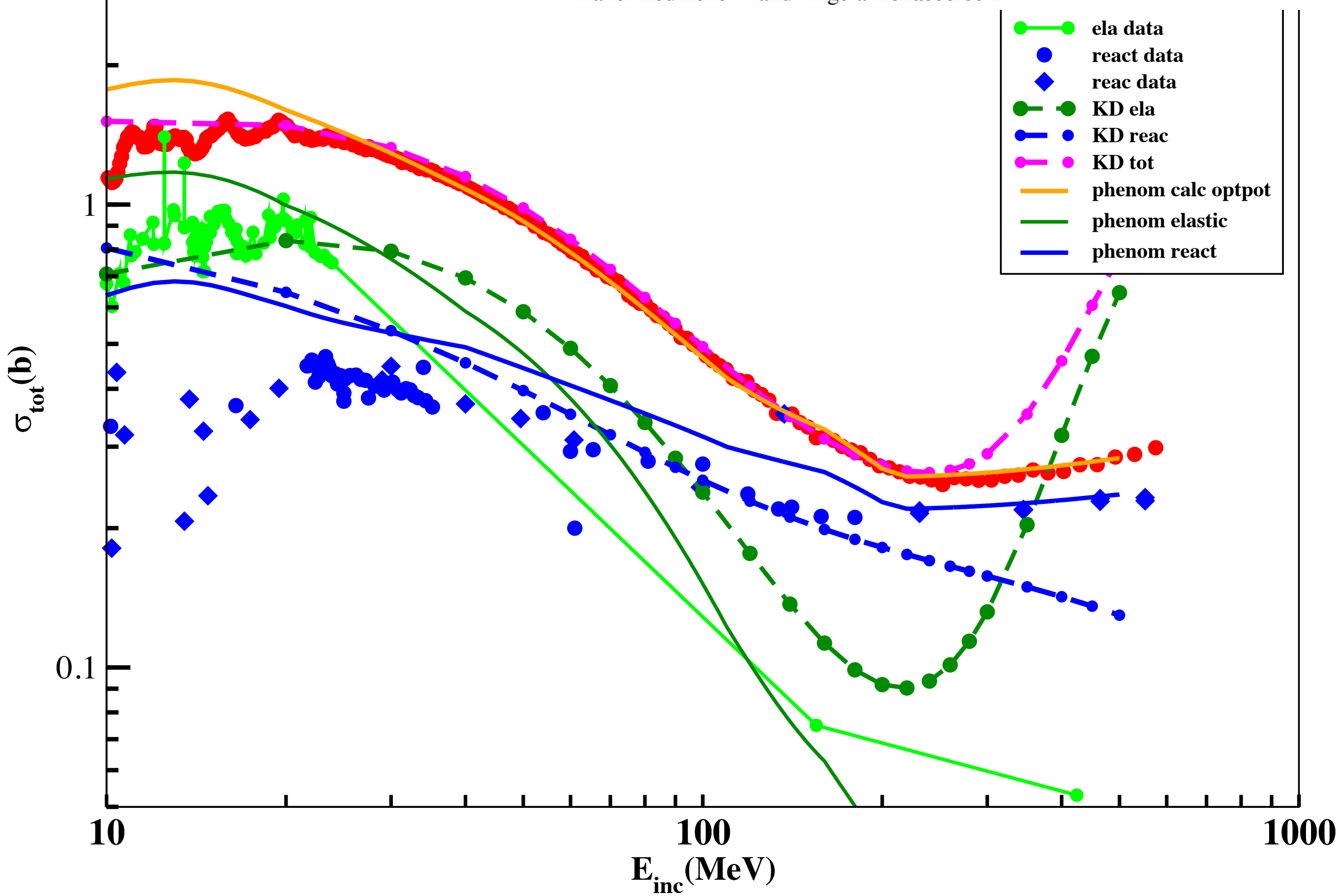

L. Ponnath et al., Phys. Lett. B 855 (2024) 138780

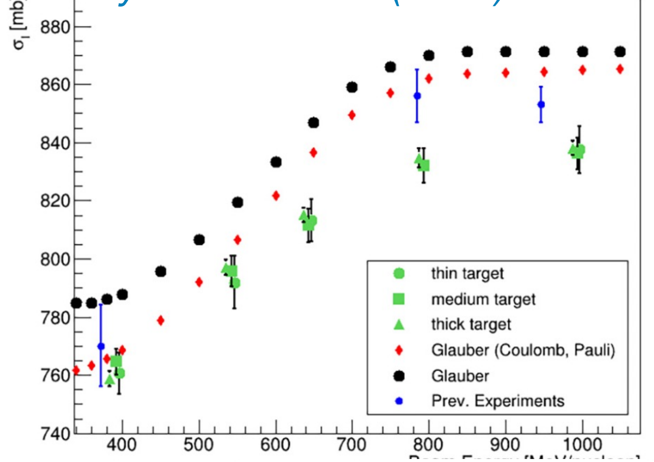

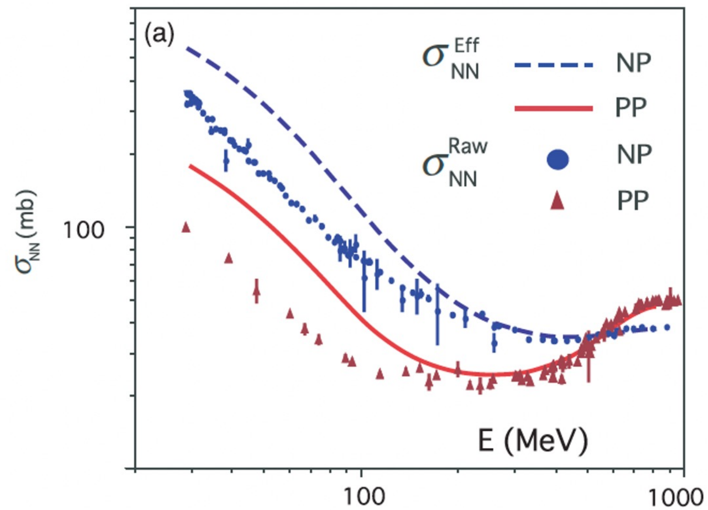

Phenomenological potentials n+^{9}Be,^{12}C

Imane Moumene & A.B. PRC108. 044609 (2023)

E_{lab} (MeV)	V^R (MeV)	r_0^R (fm)	a^R (fm)	W^{sur} (MeV)	W^{vol} (MeV)
$20\leq E_{lab} <40$	$31.304-0.145E_{lab}$	$1.647-0.005(E_{lab}-5)$	0.3-0.0001E_{lab}	$1.65+0.365E_{lab}$	$5.6-0.005(E_{lab}-20)$
$40\leq E_{lab} <111$	"	"	"	$16.25-0.05(E_{lab}-40)$	$5.5-0.01(E_{lab}-40)$
$111\leq E_{lab} <160$	"	"	0.288	12.7	4.8
$160\leq E_{lab} <200$	"	"	"	$12.7-0.025(E_{lab}-160)$	$4.8-0.025(E_{lab}-160)$
$200\leq E_{lab} <215$	"	"	"	$11.7+0.02(E_{lab}-200)$	$3.8+0.02(E_{lab}-200)$
$215\leq E_{lab} \leq 500$	0	"	"	"	"

TABLE I: Energy-dependent optical-model parameters for the (AB) potential for n+^{9}Be. r_0^I=1.3 fm, a^I=0.3 fm at all energies.

E_{lab} (MeV)	V^R (MeV)	r_0^R (fm)	a^R (fm)	W^{sur} (MeV)	W^{vol} (MeV)
$160\leq E_{lab} <200$	$31.304-0.145E_{lab}$	$1.647-0.005(E_{lab}-5)$	0.288	$12.7-0.025(E_{lab}-160)$	$4.8-0.025(E_{lab}-160)$
$200\leq E_{lab} <215$	"	"	"	11.7	3.8
$215\leq E_{lab} <220$	0	"	"	"	"
$220\leq E_{lab} \leq 500$	"	0.1	"	$11.7+0.02(E_{lab}-220)$	$3.8+0.02(E_{lab}-220)$

TABLE II: Energy-dependent optical-model parameters of the potential n-^{12}C for $E_{lab}\geq$160MeV. At lower energies, the parametrization is the same as for ^{9}Be on Table I.

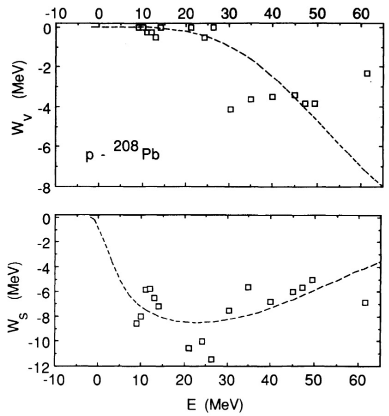

Fig. 7.29. Energy dependence of the strength of the volume and surface absorptions in the p-^{208}Pb system. The squares represent "empirical strengths" deduced from the empirical moments $[r]_W$ and $[r^3]_W$ of phenomenological optical-model potentials (Fin+ 89). The curves represent the parametrization (7.46d)–(7.46f).

Relativistic energies: Above 200 MeV both Ws and Wv increse contrary to es.

C Mahaux & R. Sartor, ADV. NUCL. PHYS. VOL. 20, (1991)

n+ ^{12}C , ^{12}C+^{12}C....

dominance of surface absorption

Total cross section for n-^{12}C scattering obtained using different target densities $\sigma_{\rho}^{s.f.}$ compared to the results obtained using the phenomenological AB potential $\sigma_{AB}^{s.f.}$ as well as the experimental value at E=300 A.MeV.

Densities / σ (mb)	HFB	HF	Wiringa	σ_{exp}
$\sigma_{\rho}^{s.f.}$	273	270	273	254
$\sigma_{AB}^{s.f.}$	257			

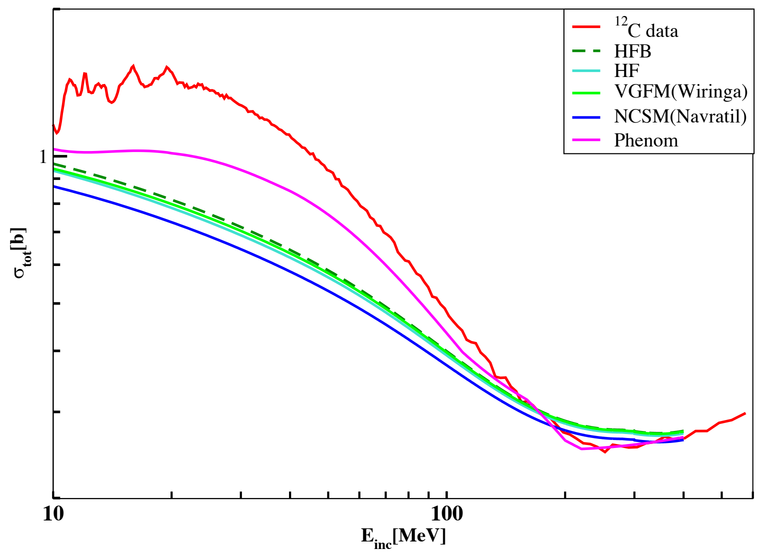

VGFM(Wiringa)

https://www.phy.anl.gov/theory/research/density/

NCSM

Ab initio no-core shell-model description of $^{10-14}$C isotopes

Priyanka Choudhary, Praveen C. Srivastava, Michael Gennari, and Petr Navrátil
Phys. Rev. C **107**, 014309 – Published 20 January 2023

Thanks to Petr Navratil and Michael Gennari for providing the numerical densities

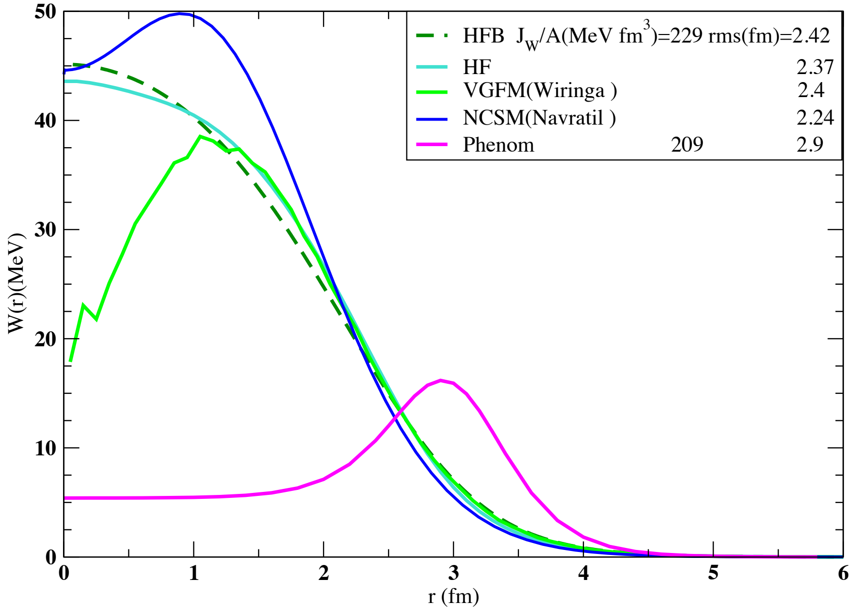

D.F. vs S.F in $^{12}C+^{12}C$

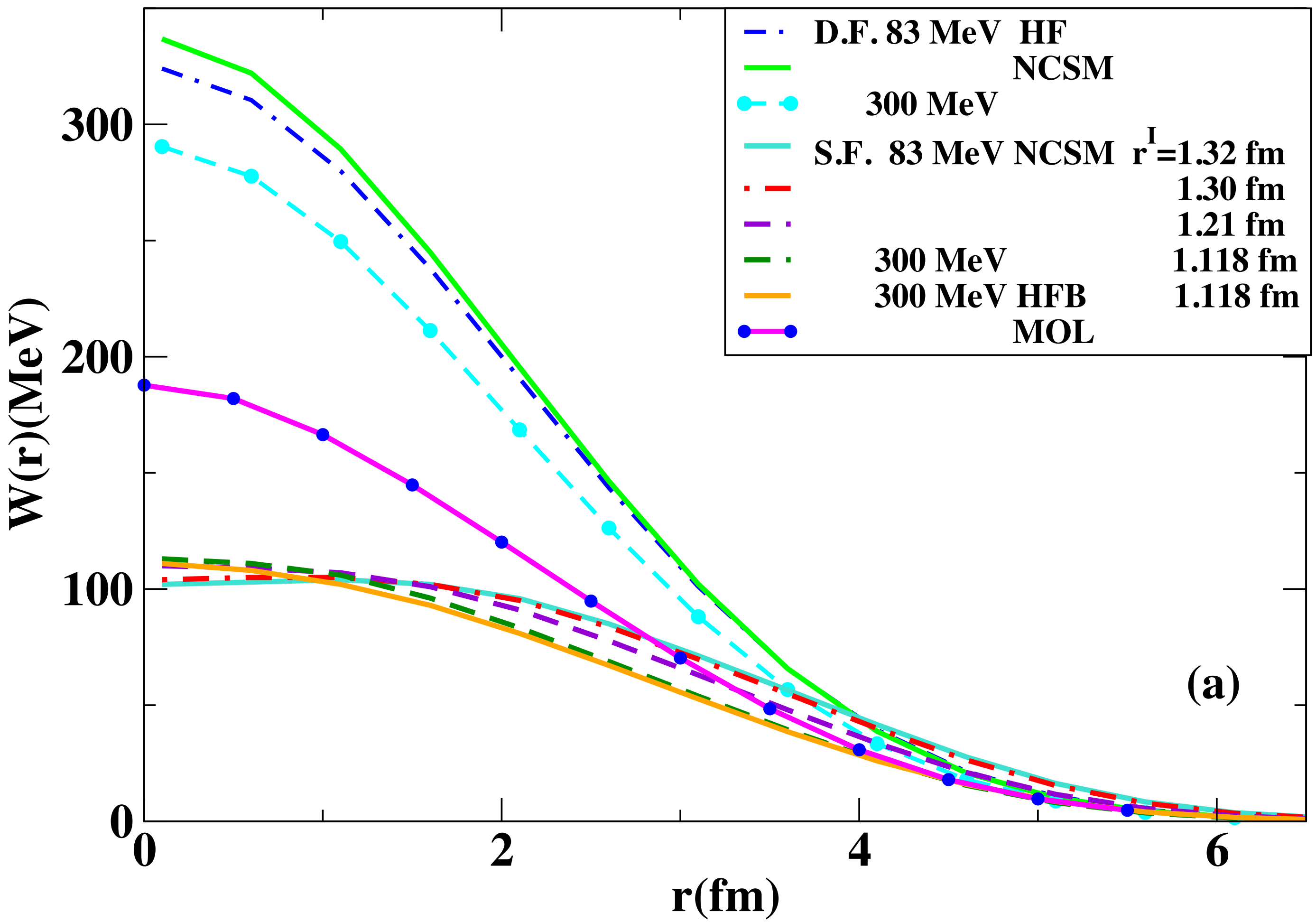

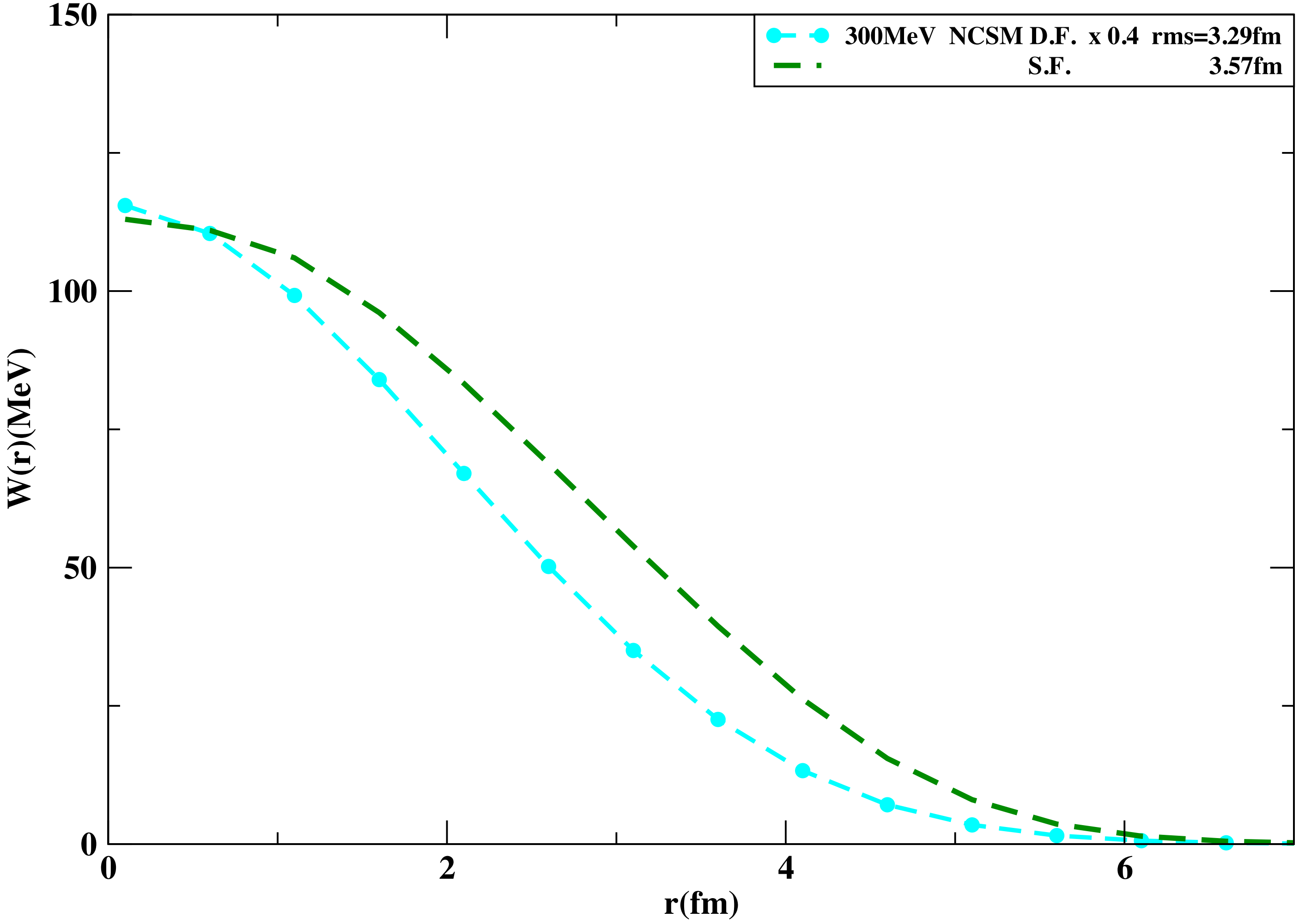

300MeV NCSM D.F. x 0.4 rms=3.29fm
S.F. 3.57fm
W(r)(MeV)
r(fm)
150
100
50
0
0
2
4
6

I. Moumene and A.B, PRC**108**, 044609 (2023)

Data from Takechi et al., Kox et al.,
In d.f. $\sigma_{np,pp}$ from De Conti&Bertulani
PRC81.064603 (2010).

E_{lab} (MeV)	$r_i(^9Be)$ (fm)	$r_i(^{12}C)$ (fm)
$30 \leq E_{lab} \leq 160$	$1.4 - 0.0015E_{lab}$	$1.32 - 0.0013E_{lab}$
$E_{lab} > 160$	1.15	1.118

TABLE III: Energy-dependent optical-model parameter r_i for the (AB) potential for n+^{9}Be and n+^{12}C

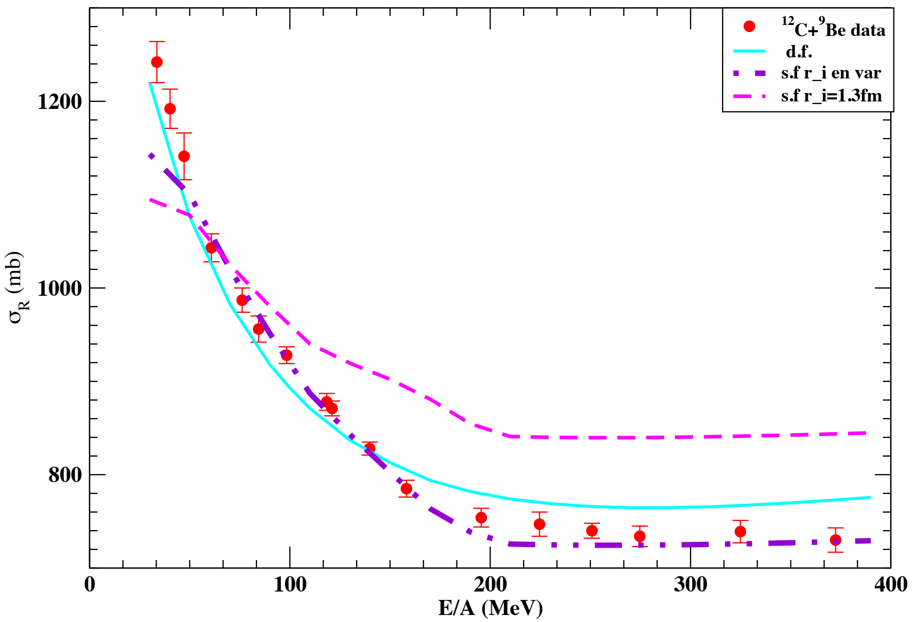

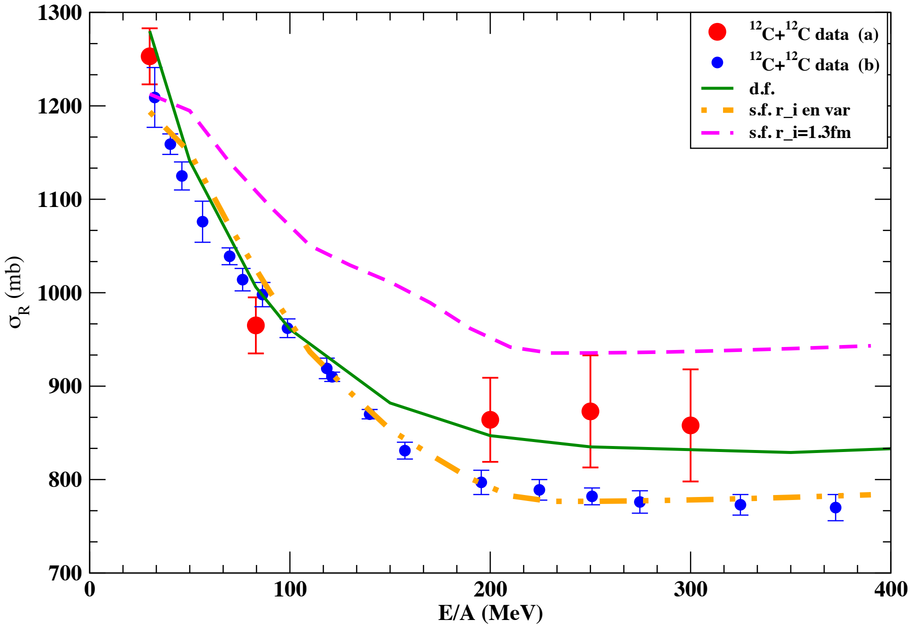

Microscopic potentials

[22] M. Burrows, C. Elster, S. P. Weppner, K. D. Launey, P. Maris, A. Nogga, and G. Popa, Phys. Rev. C **99**, 044603 (2019).
[23] A. Idini, C. Barbieri, and P. Navrátil, Phys. Rev. Lett. **123**, 092501 (2019).
[24] M. Vorabbi, M. Gennari, P. Finelli, C. Giusti, P. Navrátil, and R. Machleidt, Phys. Rev. C **103**, 024604 (2021).
[25] D. R. Entem, R. Machleidt, and Y. Nosyk, Phys. Rev. C **96**, 024004 (2017).
[26] P. Finelli, M. Vorabbi, and C. Giusti, J. Phys.: Conf. Ser. **2453**, 012026 (2023), and references therein.
[27] T. Furumoto, K. Tsubakihara, S. Ebata, and W. Horiuchi, Phys. Rev. C **99**, 034605 (2019).
[28] T. Furumoto, Y. Sakuragi, and Y. Yamamoto, Phys. Rev. C **78**, 044610 (2008).
[29] T. Furumoto, W. Horiuchi, M. Takashina, and Y. Yamamoto, and Y. Sakuragi, Phys. Rev. C **85**, 044607 (2012).
[30] W. W. Qu, G. L. Zhang, S. Terashima, T. Furumoto, Y. Ayyad, Z. Q. Chen, C. L. Guo, A. Inoue, X. Y. Le, H. J. Ong, D. Y. Pang, H. Sakaguchi, Y. Sakuragi, B. H. Sun, A. Tamii, I. Tanihata, T. F. Wang, R. Wada, and Y. Yamamoto, Phys. Rev. C **95**, 044616 (2017), and references therein.
[31] M. Toyokawa, M. Yahiro, T. Matsumoto, K. Minomo, K. Ogata, and M. Kohno, Phys. Rev. C **92**, 024618 (2015), and references therein.

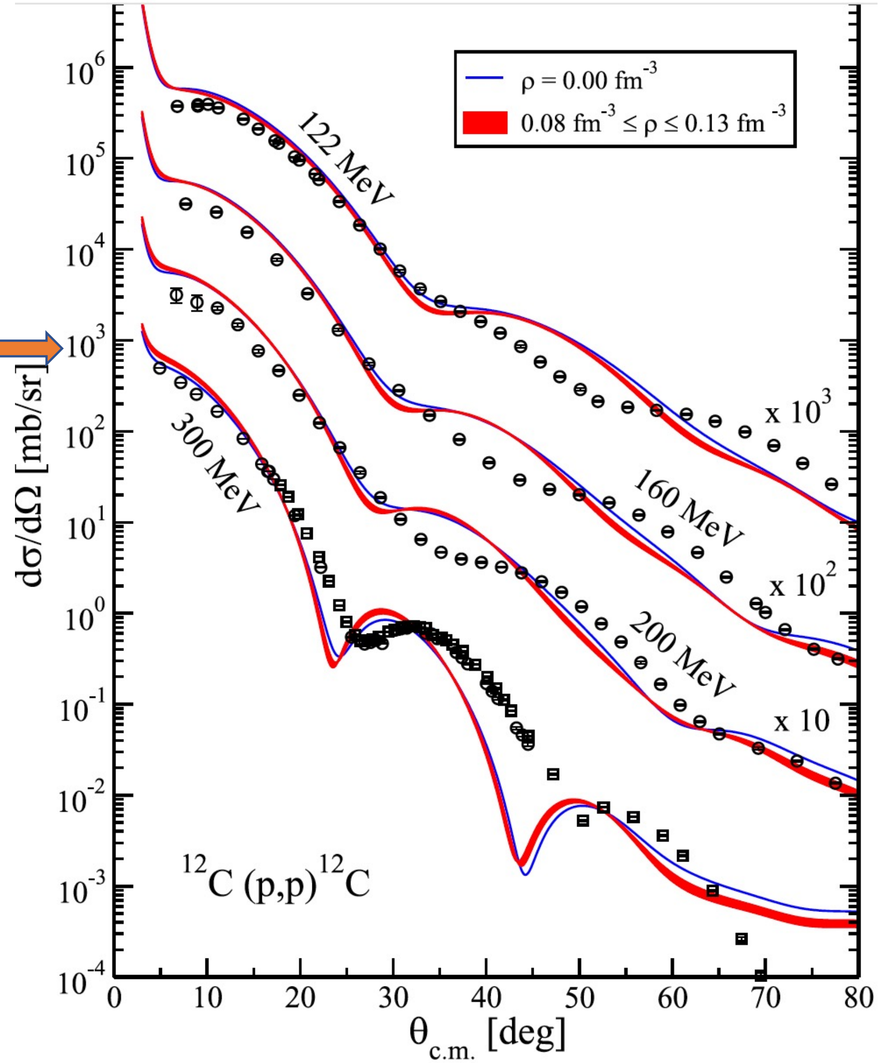

FIG. 5. The same as in Fig. 2 but for ^{12}C and for different energies (122, 160, 200, and 300 MeV). Experimental data from Refs. [83–87].

T-matrix folding vs G-matrix folding

Let us look at the future: most experiments will be at realtivistic enegies.
For theoreticians is that bad or good?

- At relativistic energy the optical limit is reached
- The optical potential should be purely imaginary
- Reaction cross section dominates
- How important is to fit elastic angular distributions?...Is it important at all?
- These seem all good news for theoreticians
- Typically increasing the energy the surface term dominates the imaginary potential for light targets
- However at relativistic energies due to the opening of new channels (π,ρ...) a phenomenological potential requires the increase of the volume term

p+12C 300MeV

H.O. Meyers et al., PRC31.1569 (1985), Okamoto et al., PRC81.*054604(2008)*

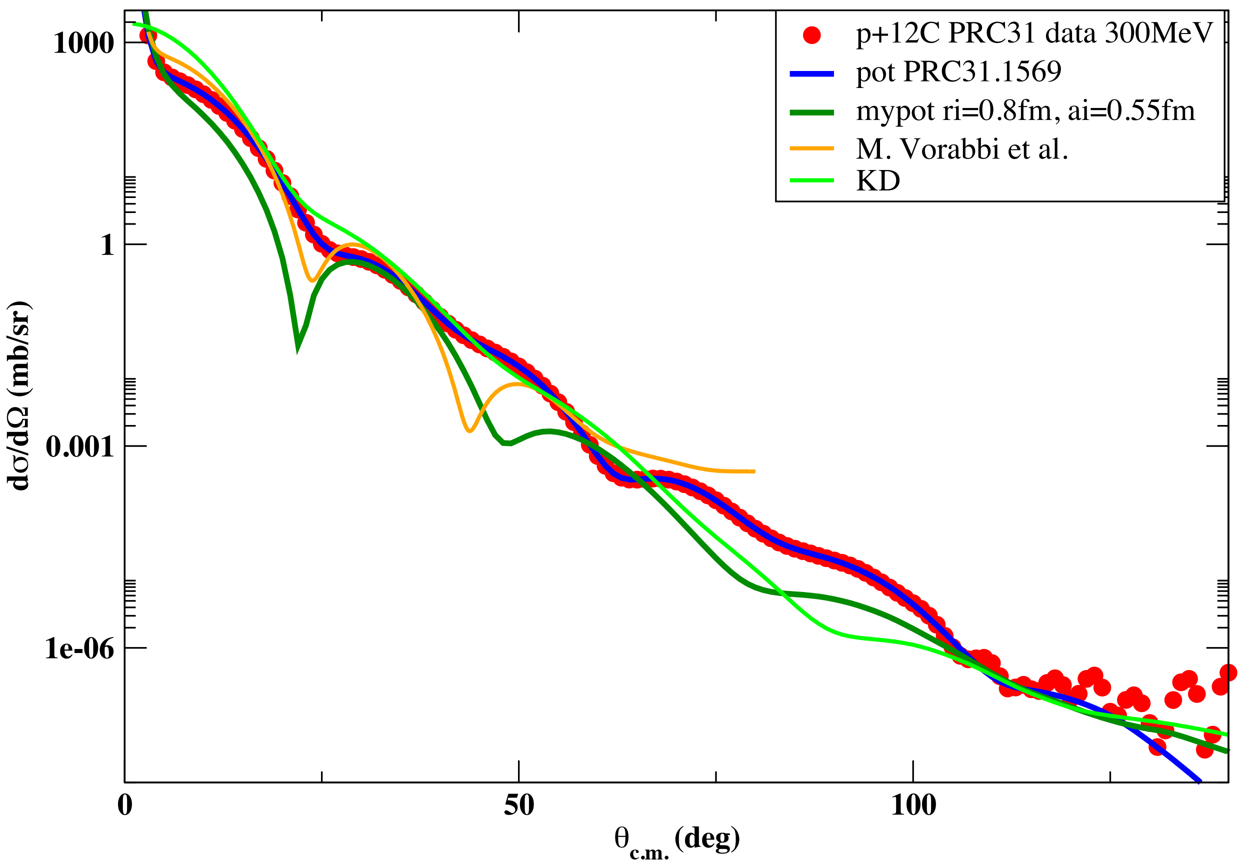

PHYSICAL REVIEW C VOLUME 31, NUMBER 4 APRIL 1985

Large-angle proton-nucleus scattering shows no evidence for intermediate Δ states

H. O. Meyer and P. Schwandt
Indiana University Cyclotron Facility and Physics Department, Indiana University, Bloomington, Indiana 47405

H. P. Gubler, W. P. Lee, and W. T. H. van Oers
University of Manitoba, Winnipeg, Manitoba, Canada

R. Abegg, D. A. Hutcheon, and C. A. Miller
TRIUMF and University of Alberta, Edmonton, Alberta, Canada

R. Helmer and K. P. Jackson
Simon Fraser University, Vancouver, British Columbia, Canada

C. Broude
Weizman Institute of Science, Rehovot, Israel

W. Bauhoff
University of Hamburg, Hamburg, West Germany
(Received 13 November 1984)

It has been suggested that the discrepancy between data for large-angle proton-nucleus elastic scattering at 200 MeV and standard optical model interpretations can be explained by the formation of intermediate Δ isobars. To test this hypothesis we have carried out a measurement of the elastic scattering cross section for 300 MeV protons from ^{12}C for momentum transfers up to 6.8 fm^{-1}. Although the energy was chosen to match the resonance energy for Δ production, no need for corrections to a simple optical model, and thus no experimental evidence for intermediate Δ isobars, was found.

Sensitivity of knockout observables to the O.P.

C. Hebborn , T. R. Whitehead , A. E. Lovell and F. M. Nunes PRC108.014601.2023

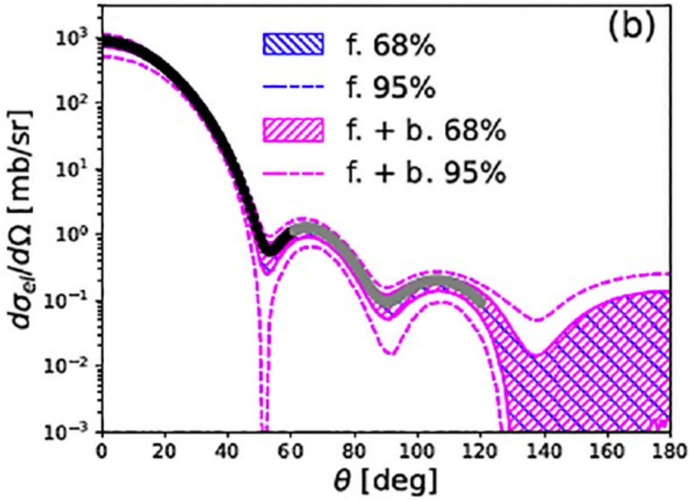

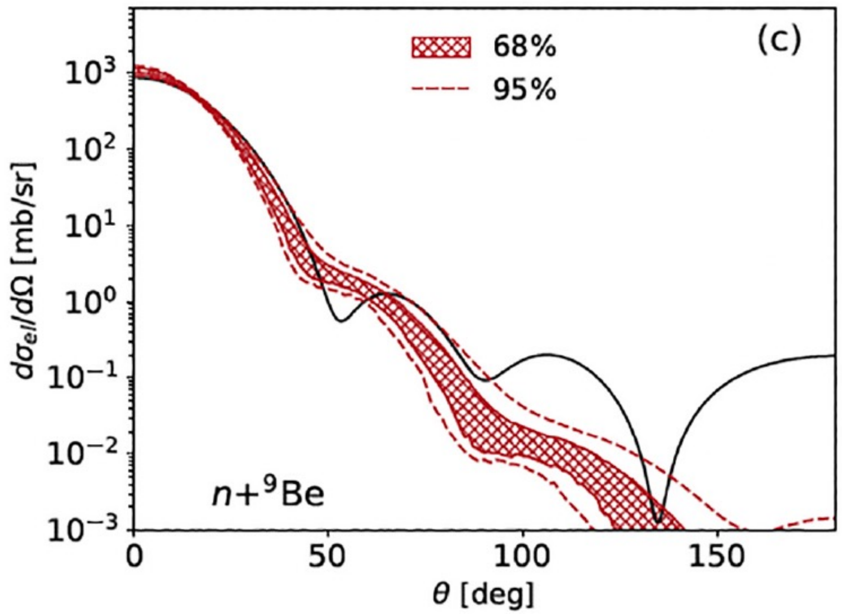

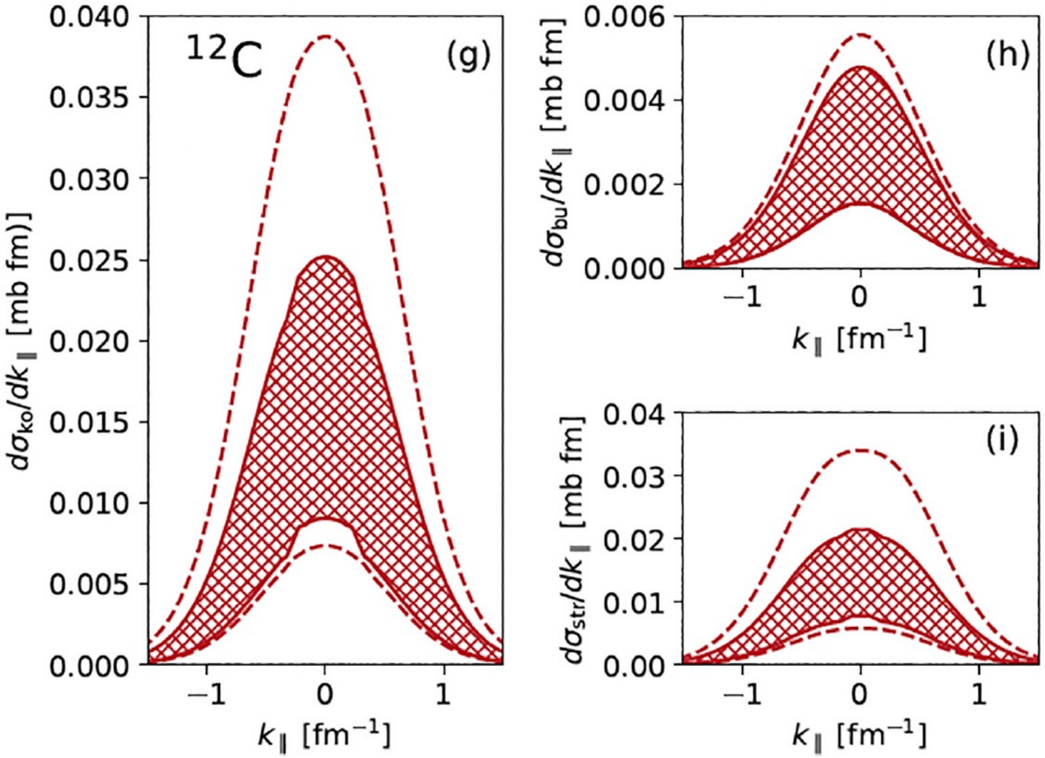

Gade-plot: reduction of S.F.

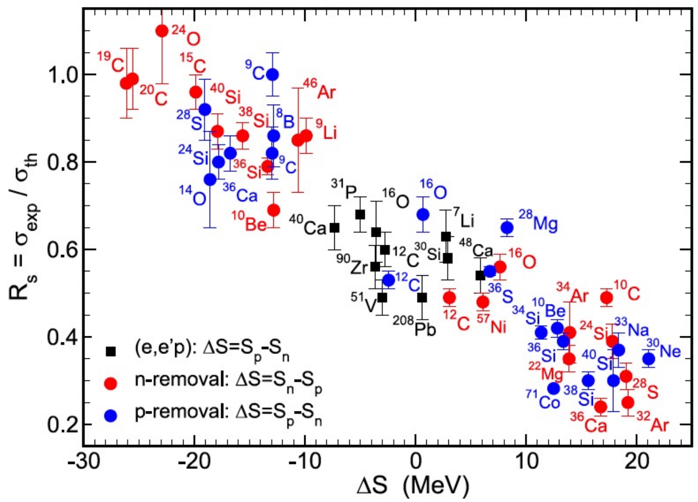

Fig. 2. Compilation of the ratios R_s of the measured and calculated inclusive one-nucleon-removal cross sections for each of the labeled projectile nuclei. R_s is displayed as a function of ΔS, a measure of the asymmetry of the neutron and proton Fermi surfaces. The red (blue) points are for neutron(proton)-removal cases. The solid (black) squares, deduced from electron-induced proton knockout data, are identical to the earlier compilations of [44,45].
Source: The figure is adapted and updated from Ref. [46] – courtesy of J.A. Tostevin (2016); the added data points for ^{24}O, ^{30}Ne, ^{33}Na, ^{36}S and ^{71}Co were then preliminary based on the now-published Refs. [47–51].

[46] J.A. Tostevin, A. Gade, Phys. Rev. C 90 (2014) 057602.
[47] I. Murray, M. MacCormick, D. Bazin, P. Doornenbal, N. Aoi, H. Baba, H. Crawford, P. Fallon, K. Li, J. Lee, M. Matsushita, T. Motobayashi, T. Otsuka, H. Sakurai, H. Scheit, D. Steppenbeck, S. Takeuchi, J.A. Tostevin, N. Tsunoda, Y. Utsuno, H. Wang, K. Yoneda, Phys. Rev. C 99 (2019) 011302.
[48] A. Gade, R.V.F. Janssens, J.A. Tostevin, D. Bazin, J. Belarge, P.C. Bender, S. Bottoni, M.P. Carpenter, B. Elman, S.J. Freeman, T. Lauritsen, S.M. Lenzi, B. Longfellow, E. Lunderberg, A. Poves, L.A. Riley, D.K. Sharp, D. Weisshaar, S. Zhu, Phys. Rev. C 99 (2019) 011301.
[49] D.A. Divaratne, C.R. Brune, H.N. Attanayake, T. Baumann, D. Bazin, A. Gade, S.M. Grimes, P.M. King, M. Thoennessen, J.A. Tostevin, Phys. Rev. C 98 (2018) 024306.
[50] J. Lee, H. Liu, P. Doornenb http://refhub.elsevier.com/ S0146-6410(21)00001-6/sb48 mo, K. Ogata, Y. Utsuno, N. Aoi, K. Li, M. Matsushita, H. Scheit, D. Steppenbeck, S. Takeuchi, H. Wang, H. Baba, E. Ideguchi, N. Kobayashi, Y. Kondo, S. Michimasa, T. Motobayashi, H. Sakurai, M. Takechi, Y. Togano, Prog. Theor. Exp. Phys. 2016 (8) (2016).
[51] A. Mutschler, O. Sorlin, A. Lemasson, D. Bazin, C. Borcea, R. Borcea, A. Gade, H. Iwasaki, E. Khan, A. Lepailleur, F. Recchia, T. Roger, F. Rotaru, M. Stanoiu, S.R. Stroberg, J.A. Tostevin, M. Vandebrouck, D. Weisshaar, K. Wimmer, Phys. Rev. C 93 (2016) 034333.

Jin Lei and A.B. PLB13.136032 (2021)
data: F. Flavigny et a., *PRL 108, 252501 (2012)*

Comparison of semiclassical transfer to continuum moc
medium energy knockout reactions

Table 1
Nucleon breakup single particle cross sections in mb for the one nucleon breakup reactions ^{14}O at 53 A.MeV and ^{16}C at 75 A.MeV on a ^{9}Be target [22]. Separation energies in MeV, asymptotic normalization constants C_i in fm$^{-1/2}$ and cross section in mb. R_f is the ratio between the experimental and IAV cross section including the shell model spectroscopic factor. Experimental and eikonal cross sections (including already the spectroscopic factors) and spectroscopic factors from Ref. [22]. See text for details.

	$S_{n(p)}$	nlj	C_i		σ_{IAV}	σ_{TC}	C^2S	σ_{eik}	σ_{exp}	R_f
^{14}O(-n)	23.12	$1p_{3/2}$	17.74				3.15			
				TOT	13.72 (6.86)	12.65		54(0.26)	14	0.3 (0.65)
				EBU	3.55	2.37				
				NEB	10.17	10.28				
^{14}O(-p)	4.63	$1p_{1/2}$	4.20				1.55			
				TOT	33.91	30.5		55(1.05)	58	1.10
				EBU	12.50	10.3				
				NEB	21.41	20.2				
^{16}C(-n)	4.25	$2s_{1/2}$	3.83				0.89			
				TOT	58.42	47.7		60(0.6)	36	0.7
				EBU	16.09	14.3				
				NEB	42.33	32.4				
	4.99	$1d_{5/2}$	0.90				0.90			
				TOT	36.29	26.9		30(1.54)	46	1.4
				EBU	10.99	7.1				
				NEB	25.30	19.8				
^{16}C(-p)	22.56	$1p_{3/2}$	19.26				2.95			
				TOT	7.45	7.48		50(0.36)	18	0.82
				EBU	1.21	1.10				
				NEB	6.24	6.38				

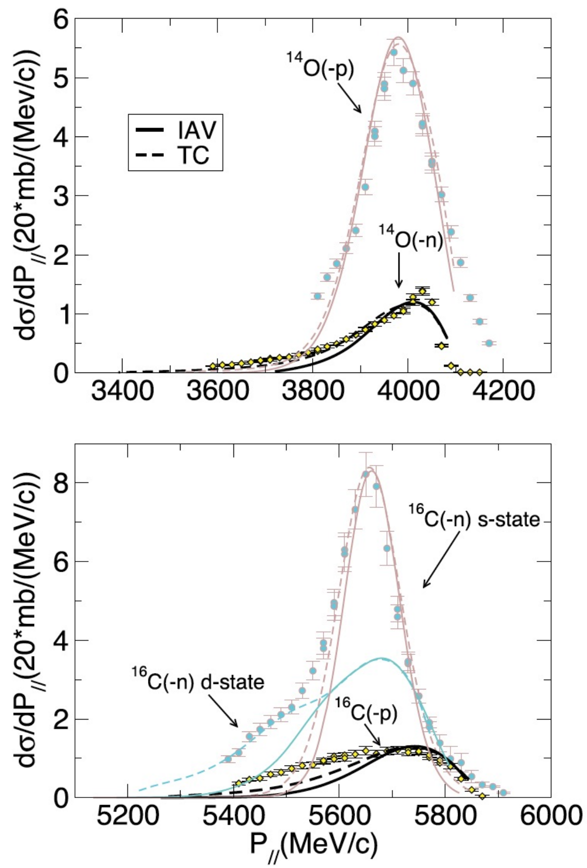

Fig. 3. Experimental and calculated cross section momentum distribution for the breakup reaction of (a) ^{14}O and (b) ^{16}C induced reactions.

Eur. Phys. J. A (2021) 57:171
https://doi.org/10.1140/epja/s10050-021-00448-1

THE EUROPEAN PHYSICAL JOURNAL A

Review

Models of breakup: a final state interaction problem

Angela Bonaccorso[1,a], David M. Brink[2]

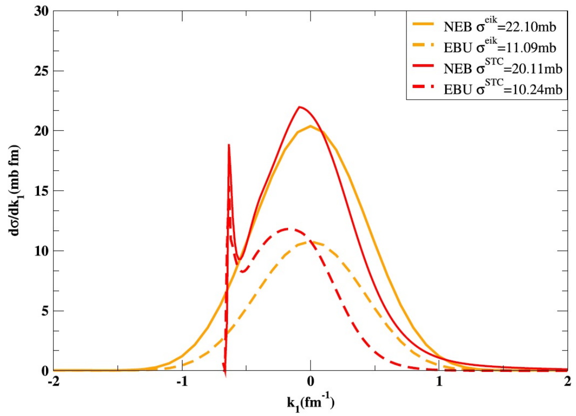

Fig. 4 Proton breakup momentum distributions in the n-Core reference frame for the reaction ^{9}Be(^{14}O,^{13}N,)X at 53 A.MeV. Red and orange curves are from the STC and eikonal models respectively. Full lines for NEB, dashed lines for EBU

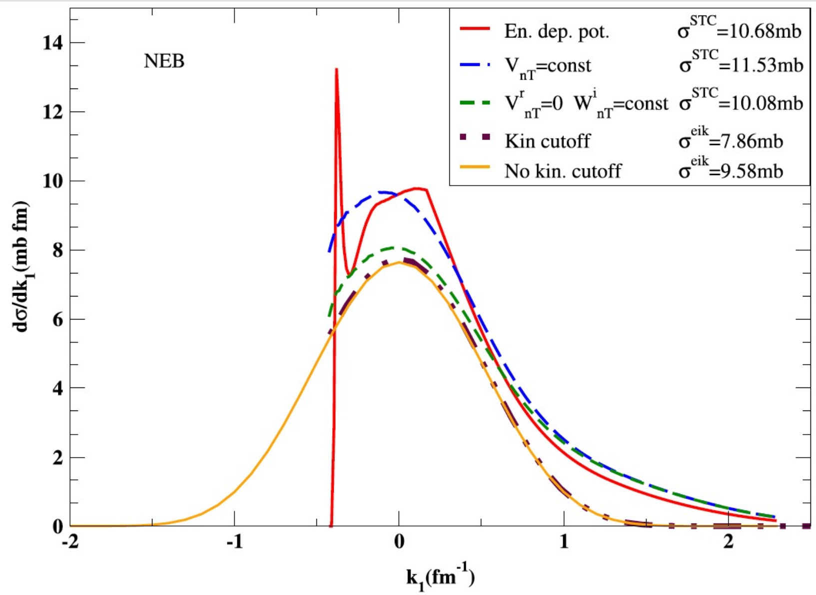

Fig. 2 NEB (stripping) neutron momentum distributions in the n-Core reference frame for the reaction ^{9}Be(^{14}O,^{13}O,)X at 53 A.MeV incident energy. The full red curve represents the STC model result, the blue long dashed curve is obtained by setting the strength of the n-T optical potential constant and equal to the value at 53 MeV, the green short dashed curve is obtained by setting the real part of the n-T potential equal to zero. The orange thin full curve shows the standard eikonal calculation, while the brown double-dotted-dashed curve shows the eikonal results in which the kinematics cutoff has been implemented. See text for more details

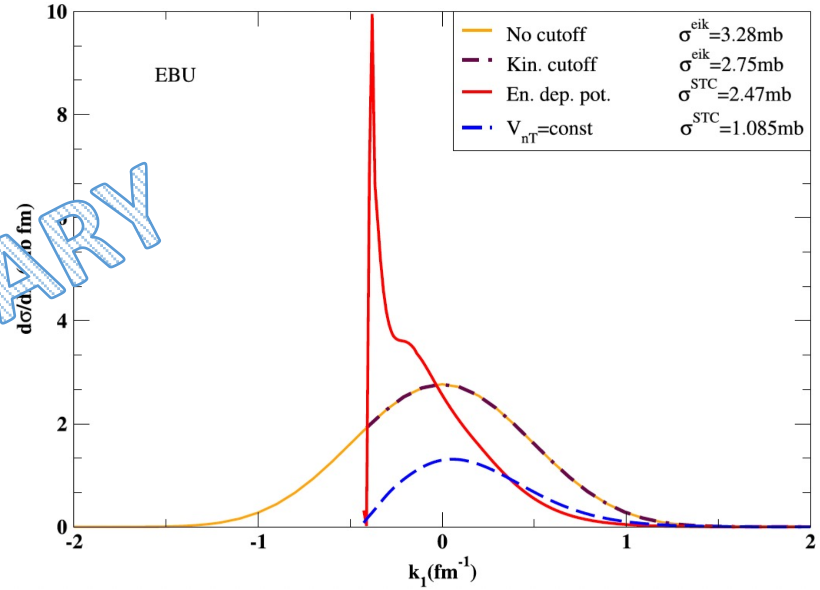

Fig. 3 Same reaction and same notation as in Fig. 2 but for EBU (diffraction) neutron momentum distributions in the n-Core reference frame. See text for more details

From PRL.108.252501: EIK: 17mb, TC 11mb

Recent results for knockout: 14O(-n)+9Be, 53AMeV WS initial wf

s.f. σ_{el}=2.89mb, σ_{abs}=7.47mb, σ_{tot}=10.37mb

d.f. σ_{el}=3.13mb, σ_{abs}=11 mb, σ_{tot}= 14.13mb

d.f. gives 30-40% larger knockout σ than s.f.

PRELIMINARY

Conclusions

- We have derived excellent n+^{9}Be, n+^{12}C phenomenological optical potentials up to 500MeV, cross checked vs DOM and n+^{9}Be also vs JLM.
- Also excellent single folding P (C)-T OP validated for ^{12}C + ^{12}C , ^{12}C+^{9}Be.
- Dominance of surface absorption (r_i decreases with energy).
- s.f. less ambigous than d.f. (needs to fix only OP parameters)
- d.f. needs σ_{np} σ_{pp} α_{np} α_{pp}…+density+in medium corrections +…??
- Extra bonus? n+^{12}C surface dominated…a symptom of 3body repulsion at short range?